Journal of Materials Chemistry B

PAPER

View Article Online
View Journal | View Issue

Cite this: J. Mater. Chem. B, 2025, 13, 15372

Discovery, biological evaluations, and modified applications of peptide AVHS derived from dental plaque biofilms

Yuan-Meng Yang,†[a] Teck-Ek Ho,†[a] Wen-Jia Gu,[b] Fei Li,[a] Edward Chin Man Lo,[c] Jian-Shu Li,[d] Jun Luo,[d] Qi Chen,[d] Lin-Lu Dai,[e] May Lei Mei,[f] Wen-Jie Zhang*[g] and Hai-Xia Lu*[a]

With the growing prevalence of early childhood caries (ECC), there is an urgent need to develop effective strategies for caries prevention. Investigation of oral metabolomic microenvironments among caries-free children could provide valuable insights. Therefore, this study aims to identify a "dominant metabolite" from plaque biofilms in children with varying levels of dental caries and to assess the biological attributes of this metabolite. A case-control study, combined with untargeted metabolomics, was conducted among three groups: caries-free (CF), low ECC (LECC), and high ECC (HECC). Then, the biological properties of this "dominant metabolite" were evaluated by biocompatibility analysis, bacterial growth and acid production assessment, biofilm targeting and remineralization test. This "dominant metabolite" was conjugated with a known antibacterial peptide Arg-Trp-Trp-Arg-Trp-Trp (RWWRWW), and the caries preventive effect of this compound was evaluated *in vitro* and *in vivo*. This study included 102 children aged 36 months. Metabolomic analysis revealed that Ala-Val-His-Ser (AVHS) was the most abundant metabolite in the CF group ($P < 0.05$), with moderate predictive performance (AUC = 0.675). AVHS has good biocompatibility; it can slow down the growth and acid production of *Streptococcus mutans* and effectively target plaque biofilm. The AVHS@RWWRWW conjugate exhibited superior antibiofilm effects *in vitro* and significantly reduced caries in rats than in the control group ($P < 0.05$). In conclusion, AVHS not only exhibits modest predictive performance for healthy children in clinical research but also demonstrates multiple biological functions. AVHS@RWWRWW shows better antibiofilm effect and can promote caries prevention, making it a promising candidate for development as a preventive agent.

Received 14th March 2025,
Accepted 24th October 2025

DOI: 10.1039/d5tb00576k

rsc.li/materials-b

1. Introduction

Early Childhood Caries (ECC), defined as dental caries occurring in children under six years of age, represents one of the most prevalent chronic childhood diseases globally.[1] The pathogenesis of ECC involves a complex interplay of multiple factors, including acidogenic bacteria, fermentable carbohydrates, and host-related factors (such as tooth morphology and salivary composition).[2,3] Left untreated, the progressive nature of ECC not only causes significant physical discomfort in affected children but also results in irreversible dental damage and negative impacts on the development of

[a] Department of Preventive Dentistry, Shanghai Ninth People's Hospital, Shanghai Jiao Tong University School of Medicine, College of Stomatology, Shanghai Jiao Tong University, National Center for Stomatology, National Clinical Research Center for Oral Diseases, Shanghai Key Laboratory of Stomatology, Research Unit of Oral and Maxillofacial Regenerative Medicine, Chinese Academy of Medical Sciences, 639 Zhizaoju Road, Shanghai 200011, China. E-mail: ritalu0225@hotmail.com
[b] Shanghai Stomatology Hospital, School of Stomatology Fudan University, Shanghai 200001, China
[c] Dental Public Health, Faculty of Dentistry, The University of Hong Kong, Hong Kong, SAR, China
[d] College of Polymer Science and Engineering, State Key Laboratory of Polymer Materials Engineering, Sichuan University, Chengdu 610065, P. R. China
[e] Department of General Dentistry, Shanghai Ninth People's Hospital, Shanghai Jiao Tong University School of Medicine, College of Stomatology, Shanghai Jiao Tong University, National Center for Stomatology, National Clinical Research Center for Oral Diseases, Shanghai Key Laboratory of Stomatology, Research Unit of Oral and Maxillofacial Regenerative Medicine, Chinese Academy of Medical Sciences, 639 Zhizaoju Road, Shanghai 200011, China
[f] Sir John Walsh Research Institute, Faculty of Dentistry, University of Otago, Dunedin 9016, New Zealand
[g] Department of Prosthodontics, Shanghai Ninth People's Hospital, Shanghai Jiao Tong University School of Medicine, College of Stomatology, Shanghai Jiao Tong University, National Center for Stomatology, National Clinical Research Center for Oral Diseases, Shanghai Key Laboratory of Stomatology, Research Unit of Oral and Maxillofacial Regenerative Medicine, Chinese Academy of Medical Sciences, 639 Zhizaoju Road, Shanghai 200011, China. E-mail: zhangwenjie586@126.com
† These authors have contributed equally to this work.

permanent dentition.[4,5] Given these substantial consequences, there is an urgent need to develop and implement more effective preventive and therapeutic strategies to address this significant public health challenge.

Recent advances in molecular biology have significantly enhanced our understanding of the composition of the oral microbiome ("Who are they?"); however, the functional aspects, particularly metabolic activities ("What are they doing?"), remain largely unexplored. Dental plaque biofilms, recognized as primary etiological agents in dental caries,[6] undergo dynamic ecological shifts driven by acidogenic and aciduric microorganisms. These microbial communities produce acidic metabolites that promote the transition to a cariogenic biofilm state, thereby playing a crucial role in caries development.[7–9] Interestingly, plaque biofilms exhibit remarkable adaptability through their capacity to counteract low pH environments by generating alkaline metabolites. Substantial evidence demonstrates that bacterial metabolic byproducts, including ammonia, putrescine, and carbon dioxide, contribute to pH neutralization within biofilm microenvironments.[10–12] This alkalization process is particularly facilitated by the metabolism of specific amino acids, such as arginine, which can be catabolized into these pH-modulating substances.[13–15] The resulting pH homeostasis in the oral microenvironment represents a critical protective mechanism against dental caries. Given the direct correlation between biofilm metabolite profiles and oral health status, current research has increasingly focused on elucidating metabolic pathways that promote biofilm alkalization and acid neutralization. This emerging focus underscores the importance of microbial metabolic activities in maintaining oral health and preventing dental caries.

The rapid advancement of metabolomic technologies has significantly enhanced our understanding of the intricate and diverse metabolic pathways operating within both microbial and host systems.[16] These technological breakthroughs have facilitated the identification of novel metabolites and biomarkers associated with dental caries pathogenesis. Notably, Schulz *et al.* employed mass spectrometry (MS)-based analytical approaches to characterize acquired pellicles in children with varying caries activity levels.[17] Their investigation revealed the presence of multiple metabolites, including short-chain fatty acids (acetic acid and propionic acid), amino acids (glycine and serine), carbohydrates (galactose, lactose, and glucose), and long-chain fatty acids (palmitic acid and stearic acid). However, the study demonstrated no significant correlation between the concentrations of these metabolites and the caries activity levels. These findings underscore the potential of metabolomics technology in elucidating differential metabolite profiles within plaque biofilms across varying stages of dental caries progression in pediatric populations.

The paradigm of contemporary caries management has evolved significantly, transitioning from traditional surgical interventions to minimally invasive medical strategies. Central to this medical approach is the utilization of bioactive materials, prompting extensive research into novel compounds with dual antibacterial and remineralization properties for effective caries management.[18] Among these bioactive agents, antimicrobial peptides (AMPs) have emerged as promising candidates. AMPs, a diverse class of host-defense molecules naturally produced by the immune systems of various organisms,[19] are represented in dental research primarily by three families: cathelicidins, defensins, and histatins. These peptides demonstrate broad-spectrum antimicrobial activity against bacteria, viruses, and fungi while exhibiting a reduced propensity for inducing antibiotic resistance compared to conventional antimicrobial agents.[20,21] Notably, LL-37, the sole human cathelicidin, exerts its antibacterial effect against *Streptococcus mutans* through membrane-interaction and pore-formation mechanisms.[22] Similarly, human beta-defensins (hBD-2 and hBD-3) have shown specific antifungal activity against *Candida albicans*.[23] Despite their potential, AMPs face several limitations that hinder their clinical application, including limited target specificity, high production costs, oral environmental instability, and potential systemic toxicity at elevated concentrations.[24,25] To address these challenges, innovative strategies, such as peptide conjugation and rational design, have been developed to enhance AMP stability and efficacy while maintaining its safety profiles.[26–28] Recent advances in machine learning have identified RWWRWW (Arg-Trp-Trp-Arg-Trp-Trp) as a potent antimicrobial peptide with remarkable activity against multidrug-resistant pathogens. However, its potential in dental caries management remains unexplored, making it an ideal candidate for conjugation studies. Therefore, this study focuses on conjugating RWWRWW with dominant metabolites to evaluate its therapeutic potential in caries prevention and management.[29]

Concurrently, the development of mineralizing peptides has emerged as a promising strategy for caries management through the induction of remineralization. Extensive research has demonstrated the significant mineralization-promoting capabilities of peptides, with particular emphasis on the critical roles of their sequence composition, net charge, and structural configuration in facilitating biomineralization processes.[30,31] Recognizing the dual functional potential of peptides in both antimicrobial activity and mineralization promotion, the investigation of multifunctional peptides represents a highly valuable research direction.

In light of these considerations, the present study was designed with three primary objectives: (1) to identify and characterize "dominant metabolites" within dental plaque biofilms from children exhibiting varying levels of dental caries through a case-control study design; (2) to evaluate the biological properties of the identified dominant metabolites, specifically focusing on AVHS; and (3) to explore their potential for modification and therapeutic application in caries management.

2. Materials and methods

2.1. The case-control study

Participants. Preschool children from Lark Kindergarten and Tomorrow Star Kindergarten in Shanghai, aged 36 months, were enrolled between March 2021 and June 2021. The children were classified into caries-free (CF), low level of early childhood caries (LECC), and high level of early childhood caries (HECC) groups. The major inclusion criteria were as follows: (i) children with no decayed teeth were classified into the CF group,

(ii) children with one to four decayed teeth in the oral cavity ($1 \leq dt \leq 4$) were classified into the LECC group, (iii) children with more than four decayed teeth ($dt > 4$) were classified into the HECC group. The other inclusion criteria were 36-month-old children living in Shanghai; children with good physical health, without hereditary diseases or deformities; and children with teeth eruption and had not using antibiotics within the last 2 weeks. Children who could not cooperate with the oral examinations were excluded. The detailed method is described in Yang Yuan-Meng *et al.*[32] This study was reported following the Strengthening the Reporting of Observational Studies in Epidemiology (STROBE) guideline.[33] The procedure of the case-control study is shown in the flowchart in Fig. 1.

This study was conducted in accordance with the Declaration of Helsinki, and ethics approval was obtained from the Ethics Committee of the Ninth Peoples Hospital, Shanghai Jiao Tong University, prior to the implementation of the study (Project identification code: SH9H-2019-A340-1), and written informed consent was obtained from the children's parents.

Sample size. The sample size was calculated by the Power Analysis module in the Metaboanalyst 5.0 platform.[34] A pilot metabolomic analysis of 10 plaque samples from 10 preschool children with and without dental caries was conducted. Ten pilot samples were excluded from the present study. A sample size of 30 was essential to satisfy 89.5% of the predicted power, with a false discovery rate of 0.05. Therefore, at least 30 children were required for each group.

Oral clinical examination and questionnaire survey. Prior to the implementation of the study, training programmes were launched to ensure reliability. Examiners availed themselves of the e-learning program on the ICDAS website to undertake relevant training for diagnosing dental caries lesions in accordance with the ICDAS standards. All the children received the oral clinical examination. The trained examiner checked the dental caries of children who were in the supine position, using a mouth mirror and Community Periodontal Index (CPI) probe under artificial light. The International Caries Detection and Assessment System (ICDAS-II) was used to record dmft scores.[35] ICDAS codes 3–6 are defined as decayed surfaces. The largest surface area was recorded when there were multiple decayed surfaces on the tooth. The decayed teeth (dt) of each child were computed according to the ICDAS scores. During the implementation of the study, 10% of the children were randomly selected for duplication on each examination day to monitor intra-examiner reproducibility, and a kappa value of 0.97 was achieved.

A questionnaire survey was conducted. Sociodemographic information, oral health-related behaviours, dietary habits, and maternal behaviours related to dental caries of children were collected through constructed questionnaires completed by their guardians.

Plaque sample collection. Supragingival plaque biofilms were collected from the children before the oral clinical examination. Sterile cotton rolls were used to block moisture, and a sterile curette in the corresponding tooth position was used to collect the supragingival plaque on each of the erupted tooth surfaces. In the caries-free group, plaque biofilms were scraped from the healthy enamel of the erupted teeth, including the buccal and labial surfaces of maxillary anterior and mandibular posterior deciduous teeth. In other groups, the surface around the dental caries was scraped. If the carious lesion was severely

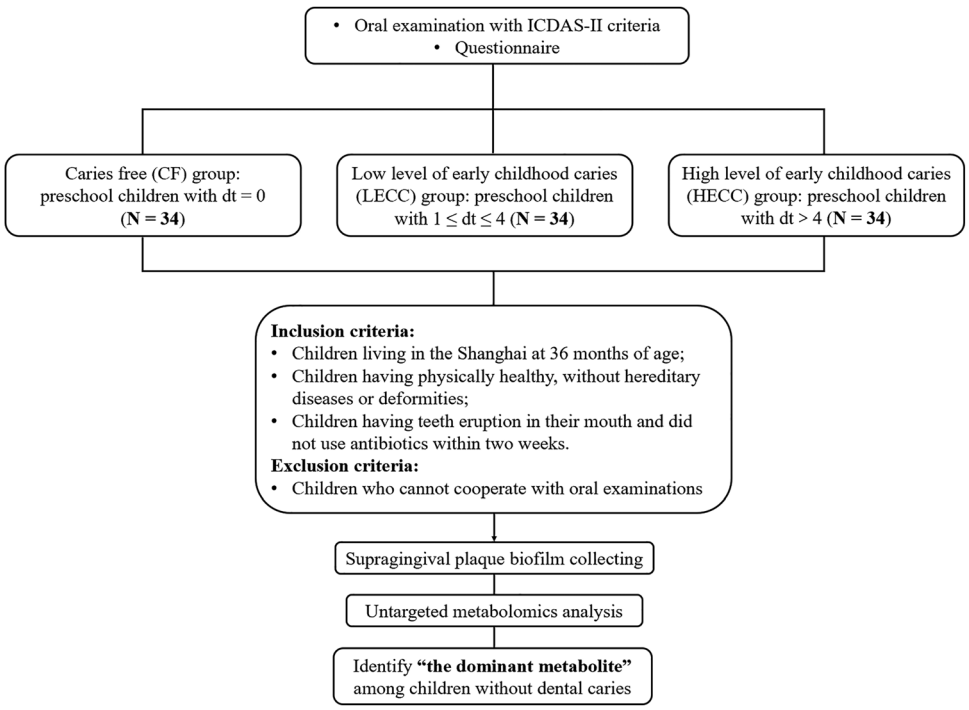

Fig. 1 Flow chart of the case-control study in the present study.

damaged, plaque biofilms were scraped from the enamel of adjacent teeth to the carious tooth. The samples were collected in sterile 1.5-mL Eppendorf tubes containing 1 mL of normal saline.

2.2. Metabolomics analysis

Metabolite extraction. The collected samples were mixed with 400 μL of the extract solution (methanol : acetonitrile : water = 2 : 2 : 1, with isotopically labelled internal standard mixture), homogenized at 35 Hz for 4 min, and sonicated for 5 min in an ice water bath. Thereafter, the samples were incubated for 1 h at −40 °C and later centrifuged at 12 000 rpm for 15 min at 4 °C. The supernatant was transferred to a fresh glass vial for further analysis. Quality control (QC) specimens were prepared by mixing equal aliquots of supernatants from all samples. The ultra-high-performance liquid chromatograph (Vanquish, Thermo Fisher Scientific, USA) containing a UPLC BEH Amide column coupled to a QExactive HFX mass spectrometer (Orbitrap MS, Thermo Fisher Scientific, USA) was used for liquid chromatography-mass spectroscopy analysis. A QExactive HF-X Hybrid Quadrupole Orbitrap mass spectrometer was used to acquire the MS/MS spectra in an information-dependent acquisition mode under the control of the acquisition software (Xcalibur, Thermo Fisher Scientific, USA).

Metabolomics data normalization. The specific data-cleaning process was as follows: 149 metabolites with relative standard deviation ≥ 0.3 and seven metabolites with more than 50% missing values were excluded from the current study. The *k*-nearest neighbour method was used to fill in the missing values of metabolites. All samples were normalized to a pooled sample from the QC group, and data were evaluated with auto-scaling to realize data normalization.

2.3. Biological properties of ''dominant metabolite''

Biocompatibility analysis. Cell proliferation and toxicity analysis were used to test the biocompatibility of the ''dominant metabolite.'' CCK-8 Kit (Beyotime, China) was applied to determine the effects of AVHS on the proliferation activity of dental pulp cells. 90 μL of a 2.0×10^4 cell suspension was seeded into a 96-well plate, and then 10-μL portions of the cell culture medium containing diverse AVHS concentrations were incorporated into each well and incubated in a 5% CO_2-containing incubator at 37 °C for 24, 48 and 72 h, followed by CCK-8-reagent incorporation and continued incubation for 4 h. The absorbance at OD_{450} was determined using a microplate reader (TECAN, Switzerland). Calcein/PI Cell Viability/Cytotoxicity Assay Kit (Beyotime, China) was used to verify the cell survival ratio. 500 μL of 2.0×10^5 cells was seeded in a 24-well plate overnight. 500 μL of the cell culture medium containing 1.25 mg mL^{-1} of AVHS replaced the medium, followed by incubation in an incubator for another 72 h. The cells were washed twice with PBS, followed by Calcein/PI-reagent incorporation according to the manufacturer's instructions and subsequent incubation for another 30 min in the dark. The samples were observed under a fluorescence microscope (Nikon, Japan).

Hemolytic activity analysis was conducted to assess the damage of the ''dominant metabolite'' on the red blood cells. Diverse concentrations of AVHS were mixed with 500 μL of 5% rabbit erythrocyte (Sbjbio, China) at a volume ratio of 1 : 1. After incubation at 37 °C for 1 h, the cells were centrifuged at 1000 rpm for 10 min. The absorbance value of the supernatant was determined at 570 nm, with the Triton X-100 (Sigma-Aldrich, Germany) addition group as the positive control and the PBS addition group as the negative control.[36] Peptides with more than 95% purity were synthesized, identified, and purified by Ketai Inc. (Shanghai, China).

Bacterial growth curve and acid production curve. The bacterial growth curve was used to profile the influence of the ''dominant metabolite'' on bacterial growth. 1.0×10^6 CFU mL^{-1} of *Streptococcus mutans* (*S. mutans*) was treated with 100 μg mL^{-1} of LL-37 and AVHS at concentrations of 5, 2.5 and 1.25 mg mL^{-1}, respectively, while the control group contained only the cell culture medium. The *S. mutans* were cultured in an anaerobic incubator at 37 °C, and samples were collected at 0, 2, 4, 6, 8, 12 and 24 h post-incubation to determine the absorbance value at OD_{600}, after which the growth curves were plotted.

The acid production curves show the influence of the ''dominant metabolite'' on the bacteria acid production. 1.0×10^6 CFU mL^{-1} of the *S. mutans* was treated with AVHS at a 1.25 mg mL^{-1} concentration. The control group contained only the cell culture medium. The *S. mutans* were cultured in an anaerobic incubator at 37 °C, and samples were collected at 0, 6, 12, 24, and 48 h post-incubation to determine the pH value using a handheld pH meter (Hengxin, China), after which the growth acid production curves were drawn.

Biofilm targeting test. A biofilm targeting test was used to evaluate the adhesion of the ''dominant metabolite'' on the biofilm. 1.0×10^8 CFU mL^{-1} of *S. mutans* was seeded in a 24-well plate after glass slides were placed in a BHI medium containing 1% sucrose (BHIS) and cultured in an anaerobic incubator for 24 h. The biofilms were rinsed three times with PBS, each time for 5 min. Rhodamine-labelled AVHS and AAAA (Ala-Ala-Ala-Ala) at the same concentrations (1 mM) were co-incubated with the biofilms for 1 h. SYTO 9 was added to stain live bacteria, followed by incubation in the dark for 15 min. The glass slides were observed under a confocal fluorescence microscope (Leica, Germany).

Remineralization test. The remineralizing effect of the ''dominant metabolite'' was determined using a pH-cycling protocol.[37] Bovine dental slices were collected and cut into $3 \times 4 \times 2$ mm^3 pieces (length × width × height) and sanded with 600, 1200, and 2000 mesh sandpapers. The dental slices were randomly divided into five groups: control (no treatment), demineralization (demineralization treatment), ddH_2O (negative control), AVHS (experiment), and casein phosphopeptide-amorphous calcium phosphate (CPP-ACP) (positive control). Except for the control group, the samples in the other groups were soaked in an acid-demineralized fluid (Xinheng, Dongguan, China) for 3 days. The acid-demineralized fluid contained 2 mmol L^{-1} calcium and phosphate and 75 mmol L^{-1} acetic acid at pH 4.3. Then, ddH_2O, 1.25 mg mL^{-1} of AVHS, and tooth mousse containing CPP-ACP (GC, Japan) were used to

treat the demineralized side of each sample for 5 min twice a day for 7 days. The samples in the above three groups underwent acid–base cycle for the remainder of the remineralization treatment, and artificial saliva (Feijing, China) was used in the base cycles. A Vickers hardness tester (Innovatest, Netherlands) was used to test the surface hardness of all samples. There were three samples in each group, and the enamel hardness values of the samples were measured and recorded post-treatment. Four sites were randomly selected from each sample; the load force was 50 g, the action time was 15 s, and the average microhardness value of the four sites was collected as the final microhardness value of each sample. Scanning electron microscopy (SEM) (ZEISS, Germany) was used to determine the surface morphology of the dental slices. Specifically, place samples directly onto a conductive adhesive, and coat the sample with gold using the Quorum SC7620 sputter coater for 45 seconds at a current of 10 mA. Capture the sample morphology using a ZEISS GeminiSEM 300 scanning electron microscope. During morphology imaging, set the acceleration voltage to 3 kV and use the SE2 secondary electron detector.

2.4. Modification application of this modified "dominant metabolite"

Biocompatibility analysis. Ala-Val-His-Ser was modified with Arg-Trp-Trp-Arg-Trp-Trp (AVHS@RWWRWW). Hemolytic activity analysis was conducted to test the damage of the modified "dominant metabolite" to red blood cells. AVHS@RWWRWW in diverse concentrations was mixed with 500 μL of 5% rabbit erythrocyte (Sbjbio, China) at a volume ratio of 1 : 1. After incubation at 37 °C for 1 h, the cells were centrifuged at 1000 rpm for 10 min. The absorbance value of the supernatant was determined at 570 nm, with the Triton X-100 (Sigma-Aldrich, Germany) addition group as the positive control and the PBS addition group as the negative control. Peptides with more than 95% purity were synthesized, identified, and purified by Ketai Inc. (Shanghai, China).

The minimum biofilm inhibiting concentration (MBIC) test. The MBIC test was used to determine the minimum concentration of the modified "dominant metabolite" required to inhibit the biofilm growth. *S. mutans* in the logarithmic growth phase was diluted to a concentration of 1.0×10^6 CFU mL^{-1} using the BHIS medium. Then, 100 μL of the bacteria solution was incorporated into each well of the 96-well plate, after which 100-μL portions of AVHS@RWWRWW at diverse concentrations were incorporated into each well. After incubating at 37 °C for 24 h, the materials were rinsed with PBS three times each for 5 min. Then, the biofilms were stained with 0.1% crystal violet for 20 min. The elution of the biofilms using 33% acetic acid determined the absorbance value at OD_{590}. SEM (ZEISS, Germany) was used to determine the surface morphology of the dental slices post-treatment with the MBIC of AVHS@RWWRWW.

Biofilm clearance tests. Biofilm clearance tests were used to determine the influence of the modified "dominant metabolite" on the formed biofilm. Five hundred microlitres of a 1.0×10^6 CFU mL^{-1} bacterial suspension was seeded in a 24-well plate after glass slides were placed in the BHIS medium. The suspension was cultured in an anaerobic incubator for 10 h, followed by rinsing with PBS three times for 5 min each. Five-hundred-microlitre portions of AVHS@RWWRWW at diverse concentrations were incorporated into each well and incubated with the early biofilms for 5 min. AVHS@RWWRWW was replaced with the BHIS medium and incubated for another 14 h. After fixation with 4% paraformaldehyde for 20 min, the biofilms were stained with 0.1% crystal violet. The biomass of the biofilms eluted with 33% acetic acid was determined using a microplate reader at OD_{590}.

Biofilm targeting test of AVHS@RWWRWW. A biofilm targeting test was conducted to evaluate the adhesion of the modified "dominant metabolite". 1.0×10^8 CFU mL^{-1} of *S. mutans* was seeded in a 24-well plate after glass slides were placed in the BHI medium containing 1% sucrose (BHIS). The bacterial suspension was cultured in an anaerobic incubator for 24 h. The biofilms were rinsed three times with PBS, each time for 5 min. Rhodamine-labelled AVHS, AAAA (Ala-Ala-Ala-Ala), AVAS (Ala-Val-Ala-Ser) and AVHS@RWWRWW at the same concentrations (1 mM) were co-incubated with the biofilms for 1 h. SYTO 9 was added to stain live bacteria, followed by incubation in the dark for 15 min. The glass slides were observed under a confocal fluorescence microscope (Leica, Germany).

Rat model of dental caries prevention. A dental caries model of rats was established. Male rats (100 ± 2 g) were purchased from Shanghai Jihui Laboratory Animal Care Co., Ltd. 10–20 mg kg^{-1} of ampicillin sodium was administered intramuscularly (i. m.) every 12 h for 3 days to eliminate oral bacteria in all rats before the formal experiment. 200 μL of the *S. mutans* (10^8 CFU mL^{-1}) suspension was inoculated on the teeth of the rats every 12 h for 3 days while feeding them with cariogenic feed and 5% sucrose water. Twelve rats were used and assigned randomly to three groups of equal numbers. Following infection by cariogenic bacteria, 200-μL portions of AVHS@RWWRWW (80 μg mL^{-1}), chlorhexidine (0.2%), and normal saline were used to treat the rats in three groups separately at 12 h intervals for 12 days. Cariogenic feed and 5% sucrose water were fed to the rats throughout the treatment period. After all treatments, the maxillaries were collected to evaluate the severity of dental caries, and the internal organs were stained with haematoxylin and eosin to determine systemic toxicity. All animals were housed under the specific pathogen-free conditions at a temperature of 22 °C to 24 °C, with stable humidity (55% ± 15%). The animal experiments were approved by the Animal Committee of Shanghai Ninth People's Hospital, Shanghai Jiao Tong University (Approval No: SH9H-2023-A86-1). The animal experiments followed the ARRIVE reporting guidelines.

The preventive effect of the drugs on dental caries was assessed using Keyes scoring. The Keyes scoring system is a traditional method used to evaluate the degree of dental caries in rats.[38] The numbers of fossae and grooves in the first, second, and third molars of the mandible were three, two,

Table 1 Characteristics of participants in the CF (n = 34), LECC (n = 34), and HECC (n = 34) groups

		CF	LECC	HECC	Total	
		N (%)	N (%)	N (%)	N (%)	P values
Socio-demographic backgrounds						
Gender	Male	11 (32.4)	14 (41.2)	18 (52.9)	43 (42.2)	0.251
	Female	23 (67.6)	20 (58.8)	16 (47.1)	59 (57.8)	
Oral-health-related behaviours and dietary habits						
Toothbrushing frequency	Once or less	18 (52.9)	22 (64.7)	13 (38.2)	53 (52.0)	0.091
	Twice or more	16 (47.1)	12 (35.3)	21 (61.8)	49 (48.0)	
Use of fluoride toothpaste*	With fluoride	13 (38.2)	6 (18.2)	12 (35.3)	31 (30.7)	0.159
	Without fluoride or don't know what fluoride is or not using toothpaste	21 (61.8)	27 (81.8)	22 (64.7)	70 (69.3)	
Last dental visit	No	25 (73.5)	29 (85.3)	20 (58.8)	74 (72.5)	0.050
	Yes	9 (26.5)	5 (14.7)	14 (41.2)	28 (27.5)	
Cleaning mouth after eating	No	11 (32.4)	12 (35.3)	5 (14.7)	28 (27.5)	0.120
	Yes	23 (67.6)	22 (64.7)	29 (85.3)	74 (72.5)	
Intake of snacks (including cakes, breads, cookies)	No	23 (67.6)	13 (38.2)	17 (50.0)	53 (52.0)	0.051
	Yes	11 (32.4)	21 (61.8)	17 (50.0)	49 (48.0)	
Maternal behaviours related to dental caries						
Mouth-to-mouth kissing children	No	25 (73.5)	22 (64.7)	26 (76.5)	73 (71.6)	0.535
	Yes	9 (26.5)	12 (35.3)	8 (23.5)	29 (28.4)	
Chewing the food before feeding it to children	No	34 (100.0)	33 (97.1)	34 (100.0)	101 (99.0)	1.000#
	Yes	0 (0.0)	1 (2.9)	0 (0.0)	1 (1.0)	

CF, caries-free; LECC, low level of early childhood caries; HECC, high level of early childhood caries; *, One missing value.

and one, respectively. The numbers of fossae and grooves in the maxillary first, second, and third molars were 2, 1, and 1, respectively. The linear scoring units assigned to each molar fossa groove were seven, five, and two in the mandible, respectively, and 5, 3, and 2 in the maxilla. The dental caries lesions were assigned four degrees: lesions that only existed in the enamel were rated as grade E. The lesions that reached the complete layer of the enamel and 1/4 of the dentin were rated as Ds. The lesions involving 1/4 to 3/4 of the dentin layer and exceeding 3/4 of the dentin thickness were rated as Dm and Dx, respectively. The dental caries in the fossae and grooves of the molars were scored to evaluate the effect of the drugs on the prevention of dental caries.

Construction of the drug intestinal response detection model. The animals received daily oral administration (200 μL per day) of AVHS (1.25 mg mL^{-1}), AVHS@RWWRWW (80 ug mL^{-1}), LL-37 (100 ug mL^{-1}), or Chlorhexidine (0.2%) for one week before being sacrificed for sample collection. Colonic samples were collected for H&E staining. Fecal samples were collected for 16S rRNA sequencing.

2.5. Statistics analysis

SPSS (version 24.0; IBM Corp., USA) was used to analyse the data. SIMCA 14.1 (MKS Instruments Inc., Sweden) and GraphPad Prism 8.0.1 were used to visualize the data. Chi-square and Fisher's exact test were used to compare differences in the sociodemographic backgrounds, oral health behaviours, and dietary habits of the children. Orthogonal partial least-squares discriminant analysis (OPLS-DA) and permutation tests were applied to evaluate the total differences between groups based on principal components. One-way ANOVA and Tukey multiple comparisons were conducted to explore significant differential metabolites among the three groups, with $P < 0.05$ set as the significance criterion. The Pearson correlation analysis was used to compute the relationships between the metabolites. A t-test was used to compare the differences between two groups. One-way ANOVA and two-way ANOVA were used to calculate the significant differences among three or more groups. Tukey multiple comparisons were performed, along with ANOVA analysis. P values under 0.05 were considered to indicate statistically significant differences.

3. Results

3.1. Participant characteristics of the case-control study

A total of 102 children (43 boys and 59 girls) were enrolled in this study and classified into three groups of 34. Table 1 depicts that there were no significant differences in sociodemographic information, oral health-related behaviours, dietary habits, or maternal behaviours related to dental caries ($P > 0.05$) among the three groups, indicating that the above information was well matched in this study. This result indicates that the three groups were comparable at the baseline in terms of key background factors that could influence dental caries.

3.2. Metabolomics profiles

A schematic diagram combining the clinical study and metabolomic sequencing is depicted in Fig. 2A. The OPLS-DA plot demonstrated significant differences among the caries-free (CF), low level of early childhood caries (LECC), and high level of early childhood caries (HECC) groups (Fig. 2B). The results of the permutation tests (200 times) demonstrated that the OPLS-DA model fit well, with $R^2 = 0.87 > 0.5$, $Q^2 = -0.608 < 0$ (Fig. 2C). The concentrations of the eighteen metabolites differed significantly among the three groups (Table 2). The heatmap depicts that AVHS (Ala-Val-His-Ser) was the most

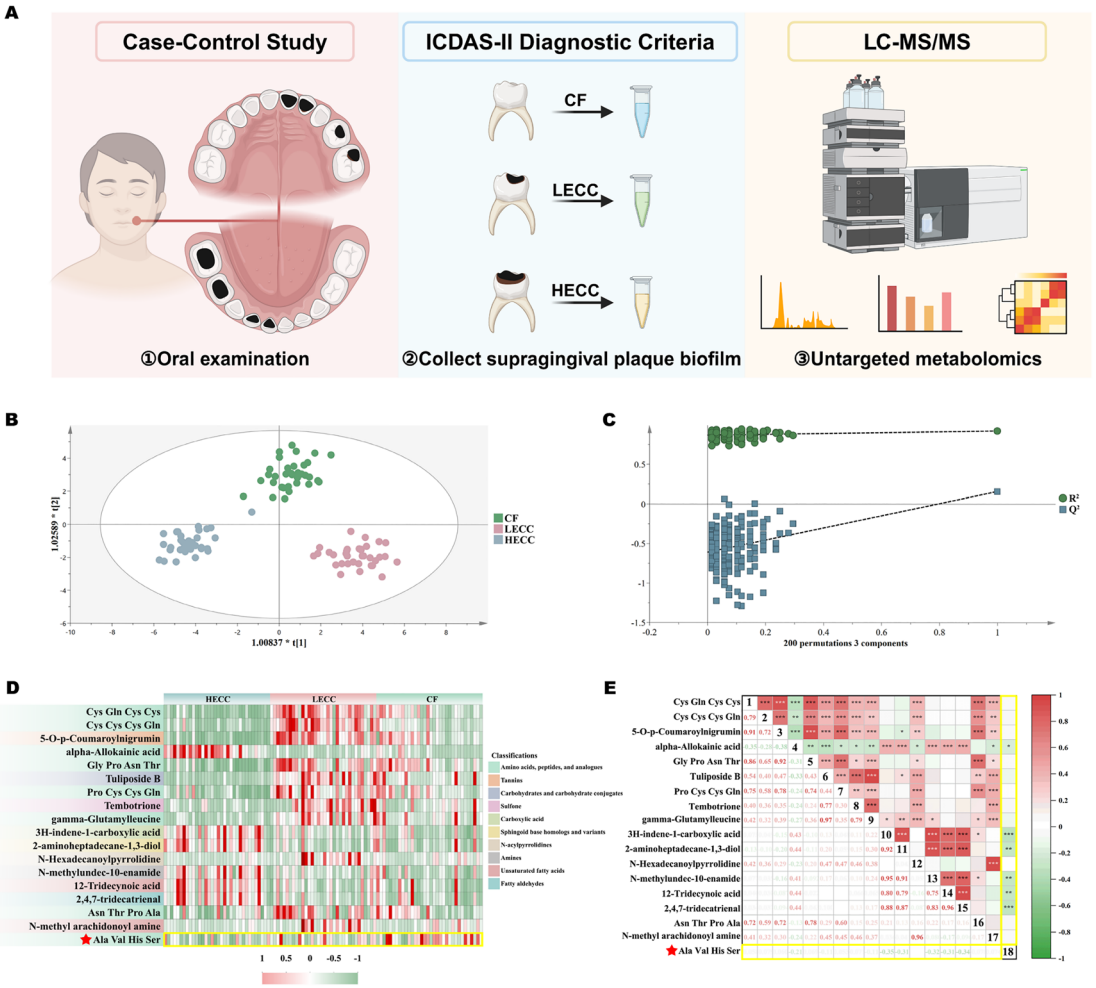

Fig. 2 Finding process of "the dominant metabolite". (A) Schematic of the finding process. (B) The OPLS-DA plot of CF, LECC and HECC groups (n = 34). (C) Permutation tests (200 times) for the OPLS-DA model. (D) Heatmap of 18 significant differential metabolites among the three groups. (E) Pearson correlation analysis of 18 significant differential metabolites (AVHS, Ala-Val-His-Ser; OPLS-DA, orthogonal partial least-squares discriminant analysis; CF, caries-free; LECC, low level of early childhood caries; HECC, high level of early childhood caries; LC-MS/MS, Liquid chromatography–tandem mass spectrometry).

abundant metabolite in the CF group among the 18 metabolites (Fig. 2D). AVHS demonstrated significant negative correlation with multiple metabolites, including alpha-Allokainic acid (r = −0.21), 3H-indene-1-carboxylic acid (r = −0.35), 2-aminoheptadecane-1,3-diol (r = −0.31), *N*-methylundec-10-enamide (r = −0.32), 12-tridecynoic acid (r = −0.31), and 2,4,7-tridecatrienal (r = −0.34), determined by *Pearson's* correlation analysis (all $P < 0.05$) (Fig. 2E). Table 3 depicts the area under the curve (AUC) values for the 18 metabolites to distinguish healthy children from children with dental caries. AVHS had the highest AUC value among other metabolites (AUC = 0.675, 95% CI = 0.56, 0.79).

3.3. Biological properties of AVHS

Biocompatibility tests of AVHS. AVHS was the most abundant in the CF group, as depicted in Fig. 3A. The structure of AVHS was depicted using the PyMol software (Fig. 3B). The three-dimensional structure shows that AVHS is composed of four amino acids: Alanine-Valine-Histidine-Serine in sequence. The stereoscopic AVHS demonstrated a linear spatial structure. The incorporation of AVHS at diverse concentrations demonstrated no significant differences from the control group during the first 3 days of cell proliferation (Fig. 3C). The results of the hemolysis experiment demonstrated that hemolysis occurred in Triton X-100 at a concentration above 0.004%, while the concentrations of AVHS from 5000 to 2.44 μg mL^{-1} did not depict any hemolysis (Fig. 3D). Triton X-100 is a non-ionic surfactant that can dissolve lipids and some membrane proteins, and molecules that can be inserted into the phospholipid bilayer and enter the cell membrane are typically believed to destroy the membrane structure.[39] Fig. 3E depicts the result of cell viability/cytotoxicity fluorescent staining. As shown in the figure, at a concentration of 1.25 mg mL^{-1}, AVHS was not toxic to the dental pulp cells, with the cell survival rate being more than 90% (92.1%), whereas the control group demonstrated an almost 90% cell survival rate (89.7%). It is generally believed that when the cell survival rate exceeds 80%, the treatment is considered nontoxic to the cell.

The bacterial growth and acid production curves of AVHS. The steps for bacterial preparation, recording of bacterial growth, acid production curves, and biofilm-targeting tests

Table 2 Significant differential metabolites of caries-free children, early childhood caries, and severe early childhood caries children's plaque biofilms

	CF	LECC	HECC		
Metabolites	Mean (SD)	Mean (SD)	Mean (SD)	*P* value	Multiple comparisons (Tukey)
Cys Cys Cys Gln	−0.29 (0.47)	1.04 (1.15)	−0.66 (0.38)	0.000	LECC > CF; LECC > HECC
Cys Gln Cys Cys	−0.05 (0.71)	0.97 (1.04)	−0.83 (0.31)	0.000	LECC > CF; LECC > HECC; CF > HECC
5-*O*-*p*-Coumaroylnigrumin	0.06 (0.73)	0.91 (1.04)	−0.88 (0.32)	0.000	LECC > CF; LECC > HECC; CF > HECC
alpha-Allokainic acid	−0.41 (0.44)	−0.50 (0.30)	1.02 (1.25)	0.000	HECC > CF; HECC > LECC
Gly Pro Asn Thr	0.27 (0.89)	0.65 (1.09)	−0.81 (0.43)	0.000	LECC > HECC; CF > HECC
Pro Cys Cys Gln	0.05 (0.76)	0.70 (1.23)	−0.66 (0.56)	0.000	LECC > CF; LECC > HECC; CF > HECC
Tuliposide B	0.08 (1.05)	0.71 (1.10)	−0.69 (0.20)	0.000	LECC > CF; LECC > HECC; CF > HECC
3*H*-indene-1-carboxylic acid	−0.39 (0.66)	−0.26 (0.55)	0.65 (1.41)	0.000	HECC > CF; HECC > LECC
Tembotrione	−0.13 (0.76)	0.73 (1.35)	−0.50 (0.36)	0.000	LECC > CF; LECC > HECC
2-Aminoheptadecane-1,3-diol	−0.26 (0.94)	−0.36 (0.60)	0.63 (1.24)	0.000	HECC > CF; HECC > LECC
N-methylundec-10-enamide	−0.34 (0.77)	−0.25 (0.50)	0.58 (1.42)	0.000	HECC > CF; HECC > LECC
gamma-Glutamylleucine	0.13 (1.15)	0.56 (1.12)	−0.58 (0.29)	0.000	LECC > HECC; CF > HECC
Ala Val His Ser	0.51 (1.28)	−0.05 (0.90)	−0.38 (0.70)	0.001	CF > HECC
N-Hexadecanoylpyrrolidine	−0.2 (0.36)	0.60 (1.63)	−0.34 (0.23)	0.000	LECC > CF; LECC > HECC
2,4,7-tridecatrienal	−0.23 (0.95)	−0.26 (0.62)	0.57 (1.27)	0.001	HECC > CF; HECC > LECC
Asn Thr Pro Ala	−0.02 (0.94)	0.55 (1.19)	−0.36 (0.74)	0.001	LECC > CF; LECC > HECC
12-Tridecynoic acid	−0.25 (1.04)	−0.26 (0.63)	0.56 (1.20)	0.001	HECC > CF; HECC > LECC
N-Methyl arachidonoyl amine	−0.15 (0.50)	0.55 (1.62)	−0.33 (0.22)	0.001	LECC > CF; LECC > HECC

CF, caries-free; LECC, low level of early childhood caries; HECC, high level of early childhood caries.

are depicted in Fig. 4A. As depicted in Fig. 4B, the growth curve of *Streptococcus mutans* (*S. mutans*) demonstrated significant differences among different groups. *S. mutans* in the control group grew rapidly and entered a stable phase after 14 h; the entire growth process exhibited an S-shaped pattern. At AVHS concentrations of 1.25, 2.5, and 5 mg mL^{-1}, the growth rate of *S. mutans* began to decrease after 2 h. Then, 1.25 mg mL^{-1} of AVHS significantly inhibited the *S. mutans* growth for 4 h, while 2.5 mg mL^{-1} inhibited it for 6 h and 5 mg mL^{-1} for 8 h ($P < 0.05$). This indicates that the lowest concentration of AVHS at which it inhibits the early growth of *S. mutans* was 1.25 mg mL^{-1}. Thus, 1.25 mg mL^{-1} of AVHS was introduced to the *S. mutans* to plot the acid production curves. LL-37 significantly inhibited *S. mutans* growth from 4 h to 24 h. In the control group, the pH decreased rapidly and reached its lowest value at 24 h. AVHS significantly inhibited early acid production, particularly during the first 24 h ($P < 0.05$). The pH during *S. mutans* acid production did not decrease to its lowest value until 48 h (Fig. 4C). Acidogenicity is related to the bacterial growth rate, as fast-growing strains metabolize sugars more rapidly and produce acidic metabolites more efficiently. Correspondingly, a low growth rate reduces acid production and thus attenuates the strain's pathogenicity.

Biofilm targeting test of AVHS. Compared to rhodamine-labelled random control peptide AAAA (Ala-Ala-Ala-Ala) (red), rhodamine-labelled AVHS (red) exhibited higher and more uniform adhesion to the biofilm (green) surface (Fig. 4D). The fluorescence colocalization results for the AVHS targeting

Table 3 Area under the receiver operating characteristic curve of 18 significant differential metabolites between children with diverse levels of dental caries

				95% Confidence interval	
Variables	AUC	Standard error[a]	Asymptotically significance[b]	Lower bound	Upper bound
Ala Val His Ser	0.675	0.059	0.004	0.560	0.790
Gly Pro Asn Thr	0.646	0.053	0.016	0.542	0.751
Tuliposide B	0.587	0.056	0.154	0.477	0.697
5-*O*-*p*-Coumaroylnigrumin	0.576	0.056	0.212	0.467	0.686
Pro Cys Cys Gln	0.570	0.056	0.253	0.459	0.680
gamma-Glutamylleucine	0.562	0.057	0.307	0.451	0.674
Cys Gln Cys Cys	0.542	0.056	0.491	0.433	0.651
Tembotrione	0.498	0.057	0.972	0.386	0.610
Asn Thr Pro Ala	0.487	0.058	0.831	0.373	0.601
N-Methyl arachidonoyl amine	0.461	0.060	0.518	0.343	0.578
N-Hexadecanoylpyrrolidine	0.454	0.060	0.452	0.336	0.572
Cys Cys Cys Gln	0.454	0.056	0.448	0.343	0.564
2,4,7-Tridecatrienal	0.353	0.060	0.016	0.235	0.471
2-Aminoheptadecane-1,3-diol	0.351	0.059	0.014	0.236	0.466
alpha-Allokainic acid	0.334	0.053	0.006	0.229	0.438
12-Tridecynoic acid	0.323	0.058	0.004	0.209	0.437
N-Methylundec-10-enamide	0.317	0.059	0.003	0.201	0.432
3*H*-indene-1-carboxylic acid	0.298	0.057	0.001	0.185	0.410

CF, caries-free; LECC, low level of early childhood caries; HECC, high level of early childhood caries; AUC, area under the curve.

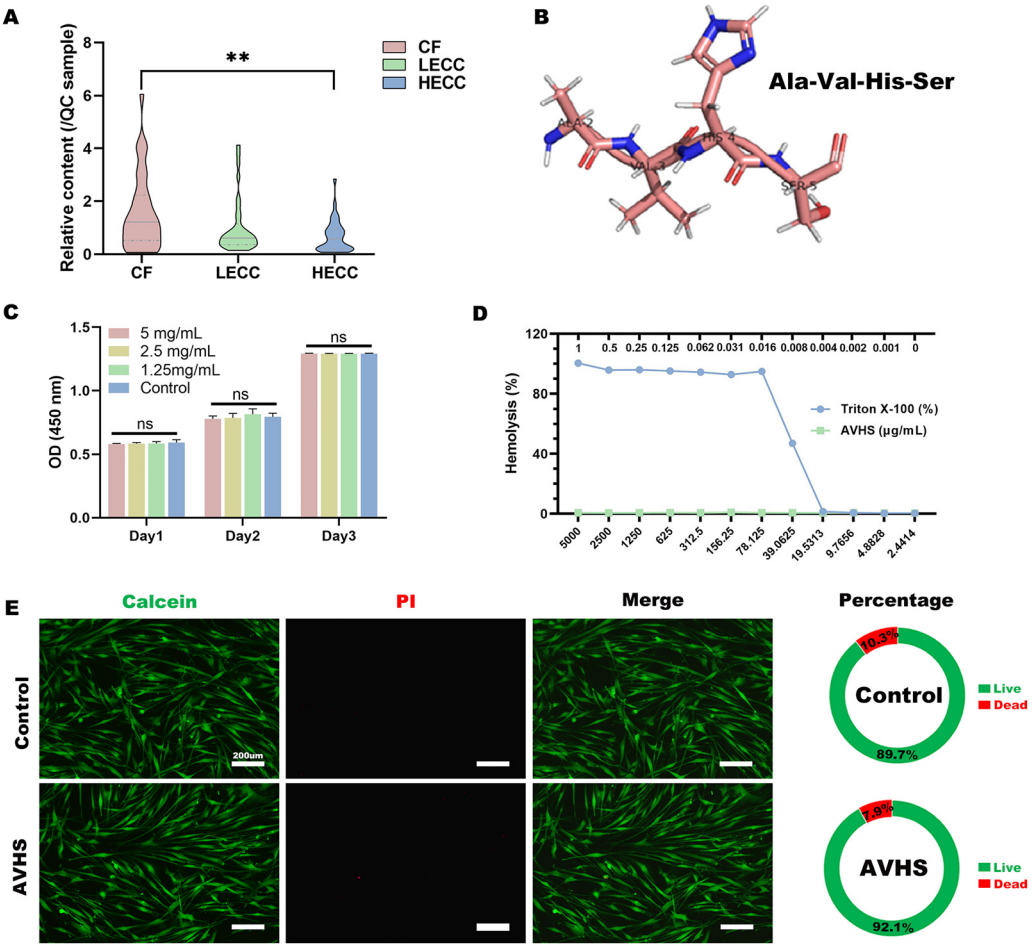

Fig. 3 Results for biocompatibility tests of AVHS. (A) Relative content of AVHS in CF, LECC and HECC groups (n = 34). (B) Stereoscopic structure of AVHS. (C) The CCK-8 results of dental pulp cells cocultured with different concentrations of AVHS (n = 4). (D) Hemolytic analysis results of red blood cells with AVHS at different concentrations (n = 3). (E) Cell viability/cytotoxicity fluorescent staining of cells cocultured with AVHS (1.25 mg mL^{-1}) (AVHS, Ala-Val-His-Ser; CCK-8, cell counting kit-8; CF, caries-free; LECC, low level of early childhood caries; HECC, high level of early childhood caries; ns, no significance).

biofilm demonstrated that the rhodamine-labeled AVHS closely tracked the green fluorescence of the biofilm. This strong overlap indicates significant colocalization between the two signals (Fig. 4E). Fig. 4F depicts the results for different concentrations of the rhodamine-labelled AVHS (1.25, 0.625, and 0.3125 mg mL^{-1}) targeting the *S. mutans* plaque biofilm. The results demonstrated that the fluorescence intensity of AVHS (red) adhered to the biofilm (green) surface increased with increasing AVHS concentration. These results indicate that AVHS can target bacterial biofilms.

Remineralization test of AVHS. Fig. 5A depicts a schematic of the remineralization process. The Vickers hardness results demonstrated that the diagonal length of the indentation formed on the surface of the demineralized tooth treated with AVHS was similar to those for the demineralized and ddH_2O groups (Fig. 5B), and there was no statistically significant difference among the three groups ($P > 0.05$) (Fig. 5C). However, the diagonal length of indentation in the control and casein phosphopeptide-amorphous calcium phosphate (CPP-ACP) groups was longer, and the Vickers hardness values of the control and AVHS groups were significantly different ($P < 0.05$) (Fig. 5B and C). Fig. 5D depicts the surface morphology of the demineralized enamel treated with AVHS, as observed by scanning electron microscopy (SEM). SEM has a three-dimensional imaging effect that offers information on the surface morphology of the substances.[40] The results indicated that the control group had a smooth surface. In the demineralized group, the surface of the enamel column was exposed in the form of non-oriented clusters with irregular shapes and uneven surfaces with large numbers of honeycomb-like pores. In the ddH_2O and AVHS groups, several pore-like structures appeared on the tooth surface, and no obvious signs of remineralization were observed. Irregular crystal deposits were formed on the surface of the dental pieces in the CPP-ACP group. In summary, AVHS did not depict obvious remineralization effects in this test.

3.4. Modification of this AVHS and its application

The biofilm targeting affinity, minimum biofilm inhibiting concentration (MBIC), biofilm clearance and biocompatibility tests of the modified AVHS. Despite that AVHS shows predictive

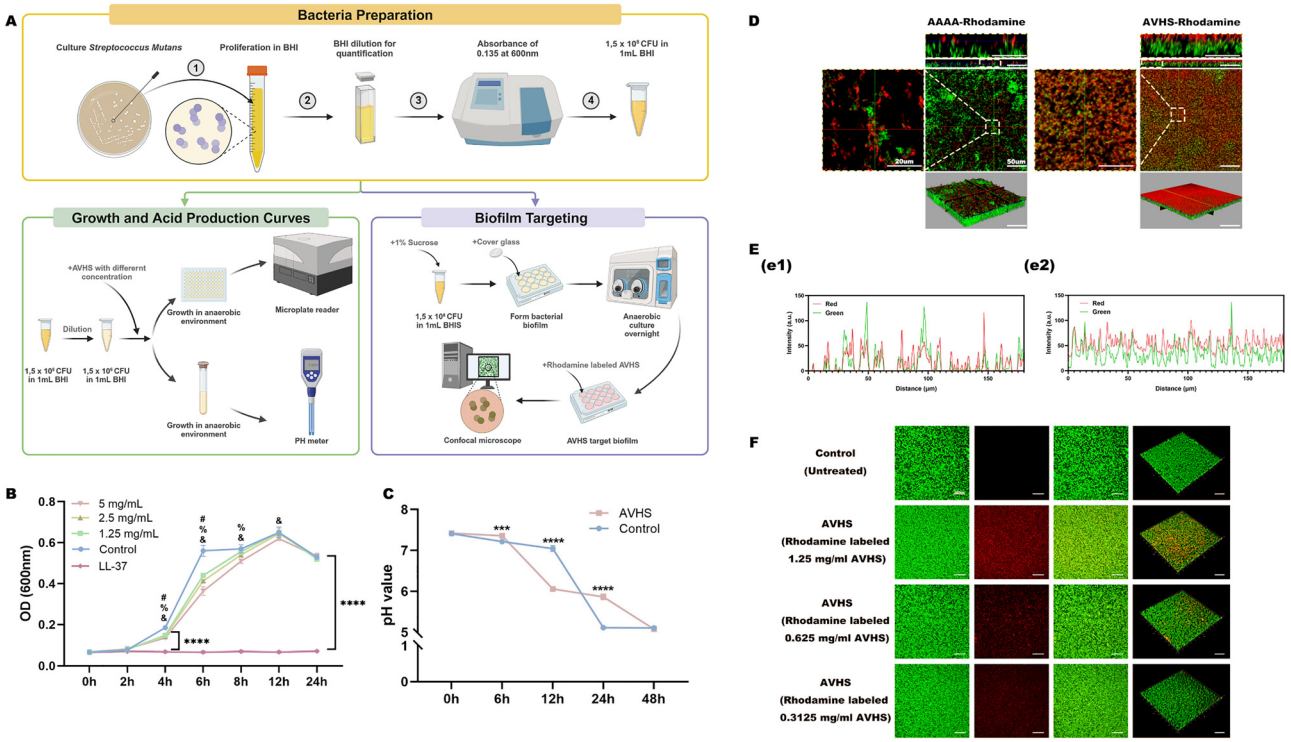

Fig. 4 Results of bacterial tests of AVHS. (A) Schematic of the bacterial test process. (B) Growth curve of *S. mutans* cocultured with AVHS and LL-37 (n = 3). (C) Acid production curve of *S. mutans* cocultured with AVHS (n = 3). (D) Biofilm targeting results of rhodamine-labeled AVHS and rhodamine-labeled AAAA. (E) Fluorescence colocalization results of AAAA-Rhodamine (e1) and AVSH-Rhodamine (e2). (F) Biofilm targeting results of rhodamine-labeled AVHS at different concentrations (AVHS, Ala-Val-His-Ser; AAAA, Ala-Ala-Ala-Ala; #, there is a significant difference between the 1.25 mg mL^{-1} group and the 0 mg mL^{-1} group; %, there is a significant difference between the 2.5 mg mL^{-1} group and the 0 mg mL^{-1} group; &, there is a significant difference between the 5 mg mL^{-1} and the 0 mg mL^{-1} groups, and the significance level of the above was 0.05; ***, $P < 0.001$; ****, $P < 0.0001$).

value for dental caries, good biocompatibility, and unique biofilm-targeting capabilities that inhibit *S. mutans* growth, its antibacterial effect was limited. To address this drawback, the AVHS was coupled with antibacterial peptides named RWWRWW, reported in the literature. Illustrations of Ala-Val-His-Ser modified with Arg-Trp-Trp-Arg-Trp-Trp (AVHS@RWWRWW) and its application in eliminating biofilms are depicted in Fig. 6A. Rhodamine-labeled peptides (AVAS, AVHS, and the modified AVHS@RWWRWW) were synthesized to assess their respective targeting and adsorption capacities. Confocal microscopy observation indicated that AVHS generated stronger fluorescence signals on the bacterial biofilm surface than AVAS. Further quantitative fluorescence analysis corroborated that AVHS possessed a superior adsorption capacity for plaque biofilms. Notably, AVHS@RWWRWW exhibited the most potent adsorption ability, as evidenced by its display of the most significant fluorescence signals on the biofilm surface (Fig. 6B and C). The minimum concentration of AVHS@RWWRWW for inhibiting biofilms formation of *S. mutans* was 40 μg mL^{-1} (Fig. 6D). Although 40 μg mL^{-1} of AVHS@RWWRWW was able to partly eliminate biofilms, 80 μg mL^{-1} of AVHS@RWWRWW, compared with other groups, demonstrated thorough biofilm elimination ($P < 0.05$) (Fig. 6E). The results of the hemolysis experiment demonstrated that hemolysis occurred in Triton X-100 at the concentration above 0.004%, while the concentrations of AVHS from 320 to 0.1536 μg mL^{-1} did not depict any hemolysis (Fig. 6F). The effects of AVHS@RWWRWW on the morphological integrity of *S. mutans* was evaluated by SEM, and the results are depicted in Fig. 6G. The biofilms that formed on the dentin slices and surfaces of *S. mutans* were smooth and remained intact in the control group (Fig. 6g1 and g2). Numerous cellular contents covered the surface without forming intact biofilms, and *S. mutans* morphology collapsed in the AVHS@RWWRWW treatment group (Fig. 6g3 and g4). The destruction of the cell's morphological integrity is associated with the leakage of cell contents and cell death.[41]

The prevention of AVHS@RWWRWW for dental caries of rats. The timeline for the development and treatment of dental caries in rats is depicted in Fig. 7A. Diverse degrees of dental caries severity were observed in the fossae and grooves of the rats (Fig. 7B). As depicted in Fig. 7C, compared to the control, both the experimental AVHS@RWWRWW ($P < 0.05$) and positive control groups (chlorhexidine) ($P < 0.01$) demonstrated a significant decrease in Keyes scores for the grade E dental caries. For grade Ds, the Keyes scores were recorded only in the fossa grooves of the control group. During this experiment, none of the drugs produced toxicity in the rat internal tissues (heart, liver, spleen, lung, and kidney) (Fig. 7D). We concluded that AVHS@RWWRWW can reduce the incidence and severity of caries in rats and has no toxic effects on the rat organs.

The protective role of AVHS@RWWRWW in intestinal health. We also investigated the effects of various antimicrobial agents on intestinal integrity and microbial composition in mice. H&E staining indicated marked intestinal wall thinning

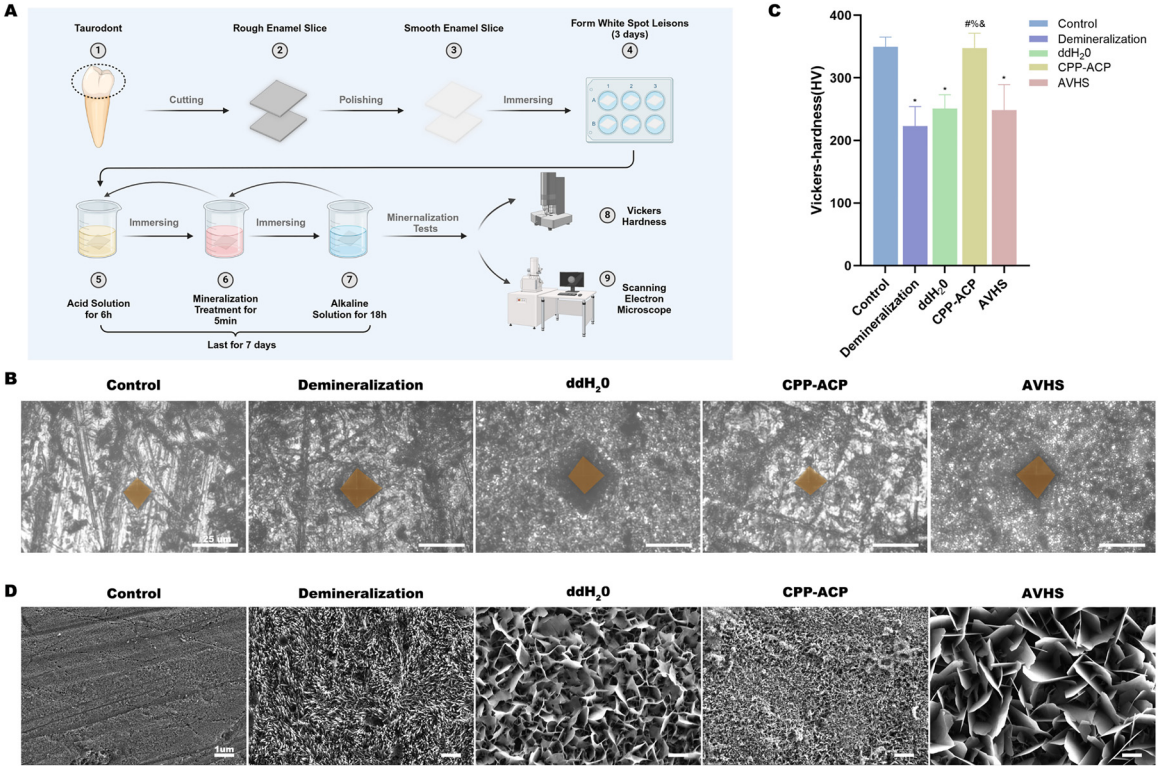

Fig. 5 Remineralization effect of AVHS. (A) Schematic of the remineralization process. (B) Representative indentation images of Vickers hardness tests with different treatments. (C) Statistical results of Vickers hardness with different treatments (n = 3). (D) Representative SEM images of enamel with different treatments (AVHS, Ala-Val-His-Ser; SEM, scanning electron microscopy; CPP-ACP, casein phosphopeptides-amorphous calcium phosphate; #, there is a significant difference between the demineralization group and the CPP-ACP treatment group; %, there is a significant difference between the ddH_2O treatment group and the CPP-ACP treatment group; &, there is a significant difference between the AVHS treatment group and the CPP-ACP treatment group, and the significance level of the above was 0.05; *, $P < 0.05$).

in the LL-37 and Chlorhexidine (CHX) groups compared to the blank control, suggesting structural impairment. In contrast, both AVHS and AVHS@RWWRWW groups showed no significant histopathological changes, indicating minimal intestinal toxicity (Fig. 8A and B).

Fecal samples were collected for 16S rRNA sequencing to assess alterations in the gut microbiota. Venn diagrams illustrated that the AVHS@RWWRWW group had the highest species richness (1845 species), with 8 operational taxonomic units (OTUs) shared across all groups (Fig. 8C). Principal coordinate analysis (PCoA) revealed that the AVHS, AVHS@RWWRWW, and LL-37 groups clustered closer to the control group, indicating relatively preserved microbial architecture, whereas the CHX group deviated significantly (Fig. 8D). Statistical analyses confirmed significant differences between all treatment groups and the control, underscoring the substantial impact of drug interventions on gut microbiota (Fig. 8E).

Pan/Core analysis was employed to examine species richness and core microbiome dynamics. At the phylum level, the AVHS and LL-37 groups exhibited compositions similar to that of the control. The AVHS@RWWRWW group showed a significant increase in Actinobacteria, while the CHX group demonstrated elevated abundances of *Bacteroidota* and *Proteobacteria* (Fig. 8F). At the species level, controls were enriched in taxa such as *s_Emergencia sp009935805*, whereas AVHS@RWWRWW led to prominent enrichment of beneficial species, including *s_Bifidobacterium globosum* (Fig. 8G). In contrast, potentially pathogenic species, such as *s_Clostridioides_A difficile*, were elevated in the LL-37 and CHX groups.

Species contribution analysis identified *s_Akkermansia muciniphila_D* as a high contributor across all five groups; *s_Unclassified_g_Blautia_A* was a major contributor in the control, AVHS, and LL-37 groups; and *s_Bifidobacterium globosum* was specifically enriched in the AVHS@RWWRWW group (Fig. 8H). LEfSe analysis further indicated that *s_Akkermansia muciniphila_D* was the most representative species in the AVHS group, *s_Bifidobacterium globosum* was the most differentially abundant microbe in the AVHS@RWWRWW group, and *s_Clostridioides_A* difficile was the most representative species in the LL-37 group (Fig. 8I).

In conclusion, AVHS@RWWRWW demonstrates not only superior biofilm-targeting adsorption but also favorable biocompatibility *in vivo*. It causes no significant intestinal damage, promotes the expansion of beneficial bacteria such as *s_Bifidobacterium globosum*, and suppresses potential pathogens, highlighting its advantages over conventional antimicrobials (LL-37 and CHX) in maintaining microbial homeostasis.

4. Discussion

This case-control study employed untargeted metabolomics to investigate the "dominant metabolite" in dental plaque

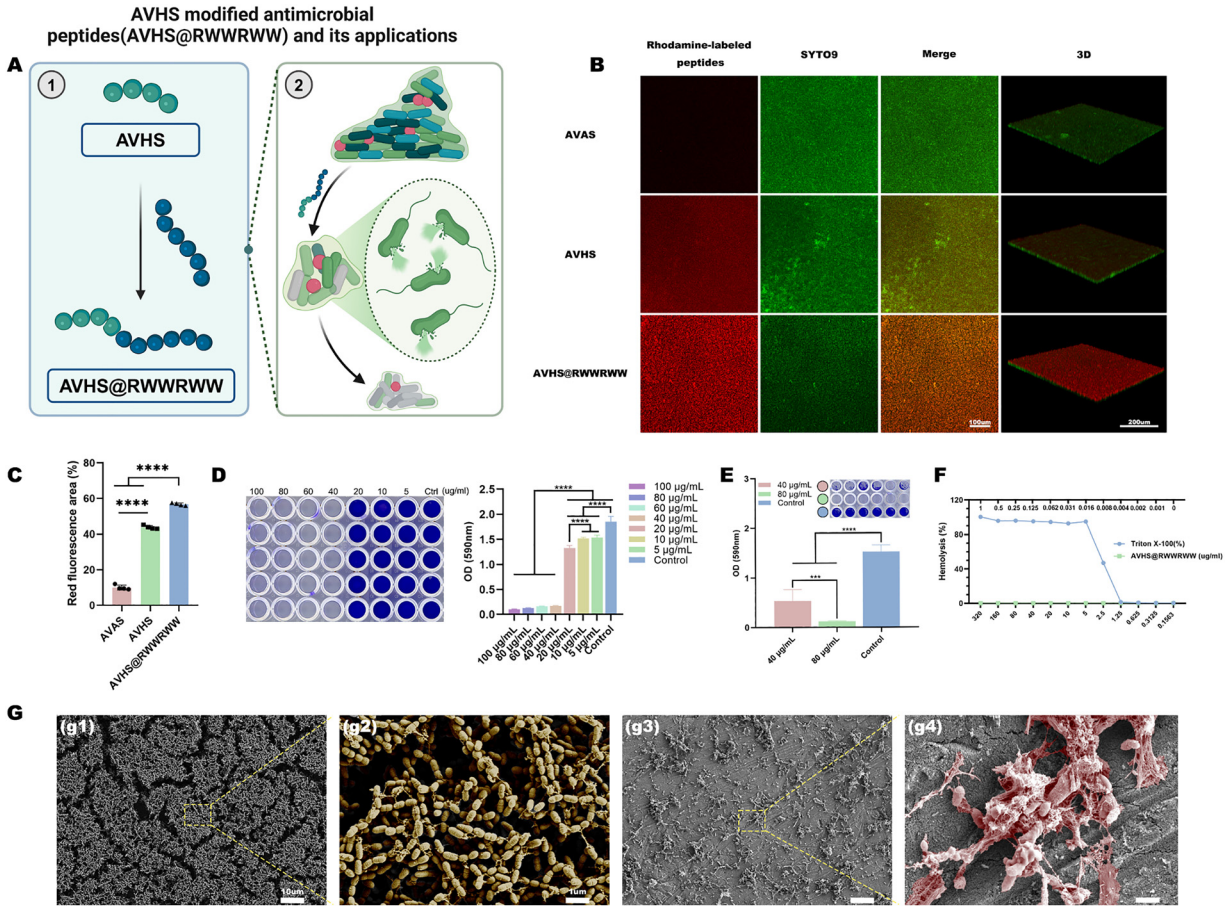

Fig. 6 Construction of AVHS modified with RWWRWW(AVHS@RWWRWW) and its anti-biofilm applications. (A) Schematic of AVHS modified with an antimicrobial peptide and its applications. (B) Biofilm targeting results of rhodamine-labeled AVHS, AVAS and AVHS@RWWRWW. (C) Statistical results of the coverage area of red fluorescence. (D) Crystal violet staining and statistical results for minimum inhibiting biofilm concentration tests of AVHS@RWWRWW (n = 6). (E) Biofilm clearance tests of AVHS@RWWRWW (n = 6). (F) Hemolysis results of red blood cells with AVHS@RWWRWW at different concentrations (n = 3). (G) Representative SEM images of *S. mutans* with different treatments. (g1): the *S. mutans* with no treatment; (g2): the enlargement image of (g1); (g3): the *S. mutans* after AVHS@RWWRWW treatment; (g4): the enlargement image of (g3); (AVAS, Ala-Val-Ala-Ser; AVHS, Ala-Val-His-Ser; AVHS@RWWRWW, Ala-Val-His-Ser-Arg-Trp-Trp-Arg-Trp-Trp; ****, $P < 0.0001$; ns, no significance).

biofilms and comprehensively evaluate its biological properties, encompassing biocompatibility, antimicrobial activity, and remineralization potential. To our knowledge, this represents the first systematic investigation of a "dominant metabolite" in plaque biofilms that potentially contributes to maintaining a healthy micro-ecological environment, with specific implications for dental caries prevention. Our metabolomic analysis identified Ala-Val-His-Ser (AVHS) as the most abundant metabolite in the caries-free (CF) group, revealing distinct metabolite profiles among children with varying caries status. Notably, AVHS demonstrated moderate predictive efficacy in distinguishing healthy children from those with dental caries. Further experimental investigations revealed that AVHS exhibits excellent biocompatibility and possesses unique biological properties, including the capacity to inhibit *Streptococcus mutans* (*S. mutans*) growth and acid production, along with biofilm-targeting specificity despite limited direct antibacterial effects. Importantly, our innovative modification of AVHS through conjugation with Arg-Trp-Trp-Arg-Trp-Trp (designated as AVHS@RWWRWW) significantly enhanced its therapeutic potential. The modified compound demonstrated remarkable efficacy in inhibiting *S. mutans* biofilm formation, disrupting established biofilms, and reducing both the incidence and severity of dental caries in a rat model. In conclusion, this study establishes a novel paradigm for dental caries management by identifying and characterizing a clinically relevant "dominant metabolite" and subsequently enhancing its therapeutic properties through targeted modification. Our findings provide a foundation for developing innovative strategies for caries prevention and oral microbiome modulation.

The initial phase of this study focused on addressing two fundamental questions in oral microbiome research: "Who are they?" by identifying key factors that contribute to maintaining the micro-ecological balance in plaque biofilms, and "What are they doing?" by elucidating their functional roles. Our investigation revealed AVHS as the predominant metabolite, showing the highest abundance in caries-free children and demonstrating moderate predictive accuracy for identifying individuals

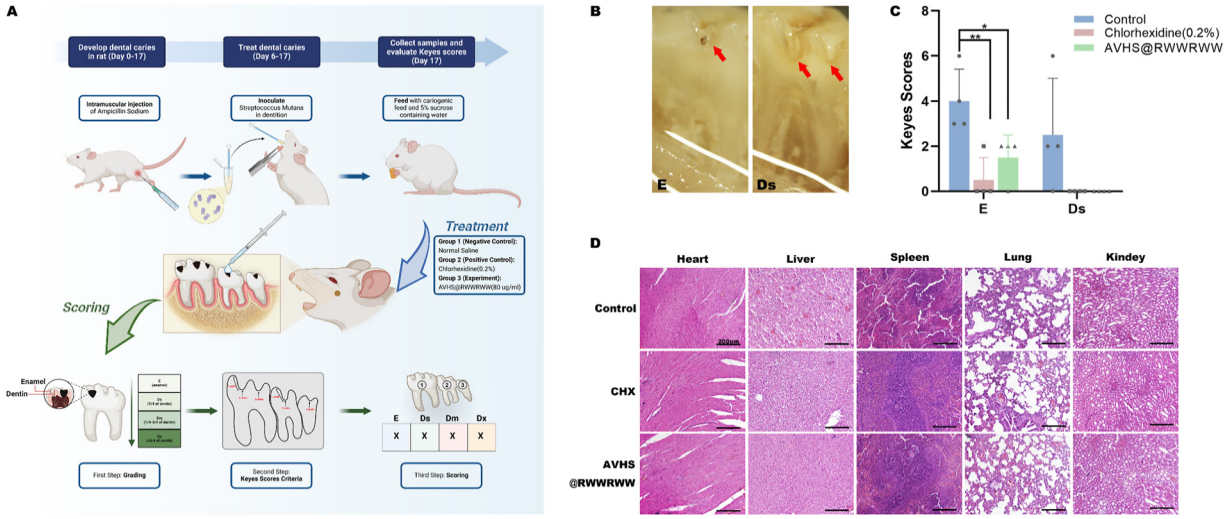

Fig. 7 Application of AVHS@RWWRWW for anticaries. (A) Schematic of developing dental caries and treatments. (B) Representative teeth images of dental caries in rats (E: grade E lesion in fossa and groove of caries; Ds, grade Ds lesion in fossa and groove of caries). (C) Keyes scores of dental caries in rats with different treatments (n = 4). (D) H&E staining for internal organs of rats with different treatments (AVHS@RWWRWW, Ala-Val-His-Ser-Arg-Trp-Trp-Arg-Trp-Trp; H&E, hematoxylin-eosin; CHX, Chlorhexidine; *, $P < 0.05$; **, $P < 0.01$).

without dental caries. This finding aligns with existing literature establishing the connection between amino acid homeostasis and oral health status,[42] where salivary amino acids and peptides serve as essential nutritional sources for supragingival plaque biofilms.[43–45] Supporting this observation, Ayad *et al.* reported elevated levels of IB-7 peptides in caries-resistant individuals compared to caries-susceptible populations.[46] The pronounced abundance of AVHS in caries-free children suggests its potential significance in maintaining biofilm homeostasis, meriting further in-depth investigation. Notably, while the tetrapeptide AVHS showed differential abundance, individual amino acids exhibited no significant variations across different caries status groups. This phenomenon may be attributed to the metabolic activities of oral bacteria, particularly those involving processes such as amino acid fermentation and decarboxylation, which could lead to the rapid depletion of free amino acids in the biofilm environment.[8]

Following the identification of AVHS in plaque biofilms, comprehensive biological evaluations revealed its multifaceted beneficial properties, including excellent biocompatibility, inhibitory effects on *S. mutans* growth and acid production, and specific targeting capability against *S. mutans* biofilms. AVHS, compared with LL-37, did not show satisfactory antimicrobial activity. This initial result led us to refine our research focus toward more specific applications where AVHS showed greater promise. Specifically, we turned our attention to its inhibitory effects on the growth dynamics of *S. mutans* and, more importantly, its ability to target plaque biofilms—a key factor in dental caries development. Indeed, the addition of AVHS significantly increased the growth period of *S. mutans* from 2 to 8 hours. Fast-growing strains typically exhibit enhanced biofilm formation, leading to increased cariogenic potential.[47,48] Therefore, slowing the early growth of *S. mutans* plays an important role in reducing its pathogenic capacity. Acidogenicity is also related to the bacterial growth rate, as faster-growing strains metabolize sugars more rapidly and produce acidic metabolites more efficiently. Correspondingly, a low growth rate reduces acid production and thus attenuates the strain's pathogenicity. As can be seen from the results, the AVHS treatment group exhibited a higher pH than the control group at 24 h. By this time, the pH of the control group had dropped below 5.5, which is the critical threshold for hydroxyapatite crystal dissolution.[49] However, the AVHS treatment group showed a slightly lower pH at 12 h; we hypothesize that this is not indicative of enhanced acidogenicity but rather a reflection of altered growth kinetics. Biocompatibility is essential for biomaterials.[50] AVHS showed no toxicity toward dental pulp-derived cells and the absence of hemolytic activity in red blood cells, underscoring its potential for clinical applications. As primary ecological determinants in caries pathogenesis,[51] oral microorganisms, particularly *S. mutans*, play a crucial role in disease progression. Our findings demonstrate that AVHS effectively modulates the cariogenic potential of *S. mutans* by attenuating its early growth phase and reducing acid production rates. This is particularly significant given that *S. mutans*, as a key cariogenic pathogen, drives caries development through carbohydrate fermentation and subsequent acid production, leading to pH reduction and disruption of biofilm homeostasis.[52] While environmental factors, such as arginine availability and fluoride concentration, are known to influence the cariogenic behaviors of *S. mutans*,[53,54] the identification of AVHS as a "dominant metabolite" introduces a novel biological factor in caries prevention strategies. The demonstrated capacity of AVHS to mitigate the pathogenic properties of *S. mutans*, coupled with its biofilm-targeting specificity, positions this metabolite as a promising candidate for developing innovative approaches in caries prevention and oral microbiome modulation.

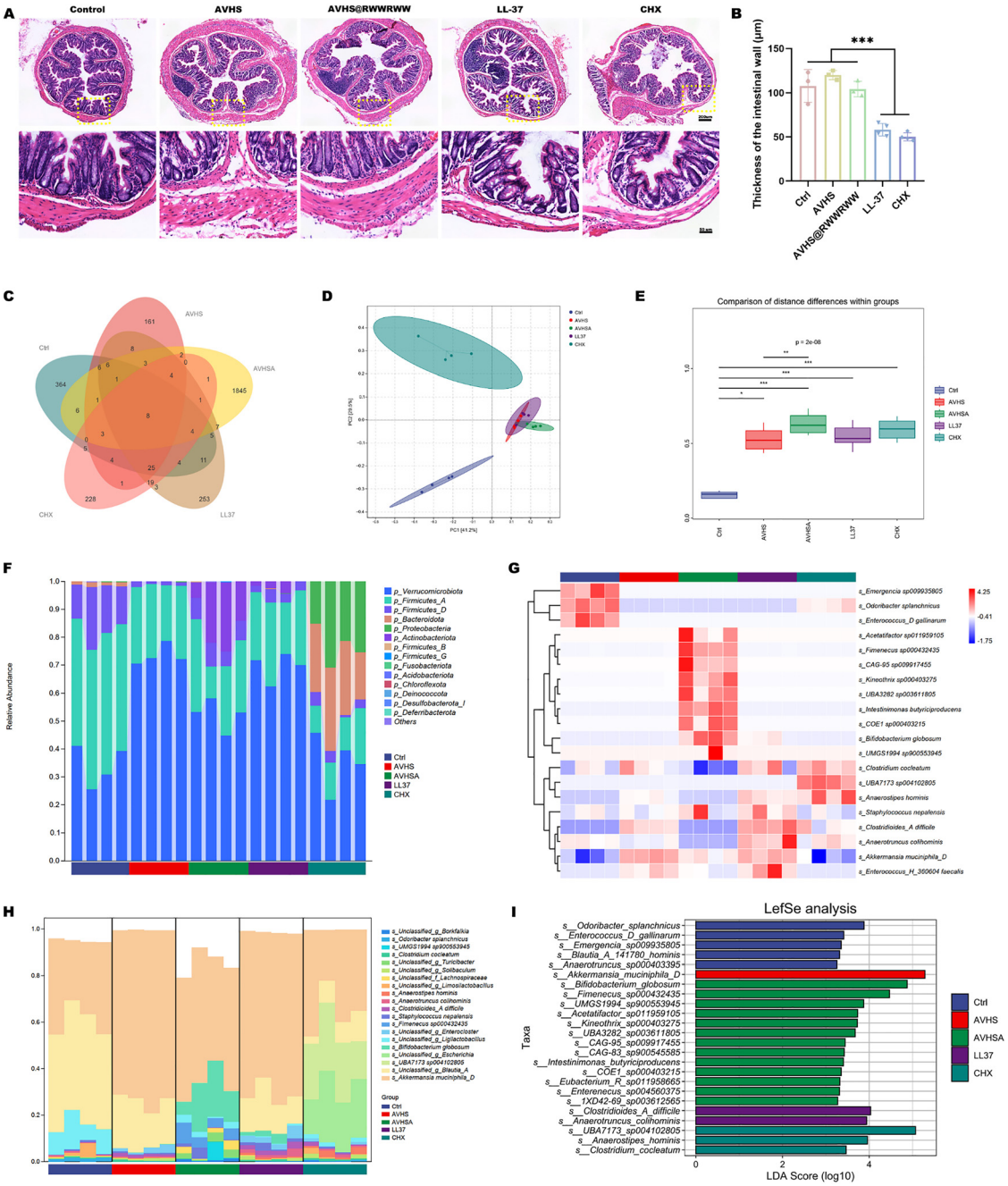

Fig. 8 Protective role of AVHS@RWWRWW in intestinal health. (A) HE of colon. (B) Thickness of the colonic intestinal wall. (C) Venn plot of all groups. (D) PCoA of all groups. (E) Comparison of distance within groups. (F) Taxa composition in the phylum. (G) Heatmap of taxa composition in species. (H) Species contribution of all groups. (I) LefSe analysis of all groups (AVHSA, abbreviation of AVHS@RWWRWW, Ala-Val-His-Ser-Arg-Trp-Trp-Arg-Trp-Trp; H&E, hematoxylin-eosin; CHX, Chlorhexidine; *, $P < 0.05$; **, $P < 0.01$).

Dental plaque biofilms serve as complex biological matrices that anchor microbial communities to tooth surfaces and mediate intricate microorganism-host interactions. The nature of these interactions determines the ecological balance, potentially promoting oral health or predisposing to dental caries development.[55] This dualistic role underscores the critical function of plaque biofilms in creating a unique microenvironment that influences microbial survival dynamics and caries pathogenesis. Our biofilm-targeting experiments revealed that AVHS exhibits significant affinity for bacterial biofilms. The effective targeting of biofilms typically requires specific structural characteristics, such as nanoscale dimensions or the capacity for electrostatic interactions with anionic biofilm components and bacterial membranes.[56–58] AVHS possesses both crucial properties: its tetrapeptide structure provides an optimal molecular size, while the presence of histidine residues confers a weak positive charge. This structural configuration likely facilitates electrostatic interactions with negatively charged extracellular polysaccharides

and bacterial cell surfaces, potentially explaining the effective biofilm targeting capability of AVHS. However, the precise molecular mechanisms underlying this targeting phenomenon warrant further systematic investigation to fully elucidate the structure–function relationship.

The progression of dental caries involves a dynamic equilibrium between demineralization and remineralization processes. When this balance is disrupted, persistent demineralization can lead to the formation of white spot lesions, characterized by surface roughness and increased porosity, which represent the initial clinical manifestation of caries development.[59] In our experimental investigations, while AVHS treatment failed to demonstrate significant remineralization potential, casein phosphopeptides-amorphous calcium phosphate (CPP-ACP) exhibited remarkable efficacy in promoting enamel remineralization. The superior remineralization capability of CPP-ACP can be attributed to its unique biochemical properties. CPP-ACP complexes dissociate into bioavailable calcium and phosphate ions, creating a sustained supersaturated state at the enamel surface that facilitates the repair of demineralized lesions.[60] This mechanism of action establishes CPP-ACP as a highly effective remineralizing agent, particularly valuable for managing early caries lesions and preventing their progression.

Dental caries represents a chronic biofilm-mediated infectious disease, with dental plaque biofilms serving as the primary etiological factor.[61] Conventional approaches to managing biofilm-associated infections typically combine mechanical biofilm disruption with antimicrobial agents to eradicate pathogenic bacteria.[62–65] However, the inherent resistance of biofilm-embedded microorganisms, which can be up to 1000 times more than their planktonic counterparts, presents significant therapeutic challenges.[66–68] This problem is further exacerbated by the global rise in antimicrobial resistance due to the widespread use of antibiotics and other antimicrobial agents.[69] Given the pivotal role of dental plaque biofilms in caries pathogenesis and their function as protective barriers for cariogenic bacteria, effective biofilm elimination should be a cornerstone of caries prevention and treatment strategies. In this study, we developed an enhanced therapeutic agent by conjugating AVHS with RWWRWW (designated as AVHS@RWWRWW). This novel compound demonstrated remarkable efficacy in both inhibiting and eradicating bacterial biofilms while significantly reducing caries incidence in a rat model. The therapeutic effect of AVHS@RWWRWW was comparable to that of chlorhexidine, a gold-standard antimicrobial agent commonly incorporated in oral care products, such as mouthwashes and dental primers.[70,71] AVHS@RWWRWW demonstrated an excellent safety profile, showing no evidence of systemic toxicity in vital organs while maintaining potent anti-caries efficacy. These findings position AVHS@RWWRWW as a promising alternative antimicrobial candidate that combines therapeutic effectiveness with enhanced safety. Further investigations are warranted to fully explore the clinical potential of this innovative compound. The current investigation focused on supragingival plaque biofilms as a model system to identify and characterize the "dominant metabolite" associated with caries prevention. As complex micro-ecosystems, plaque biofilms play a pivotal role in caries pathogenesis and represent an ideal environment for studying microbial metabolites.[7,72]

Different drug treatments caused significantly diverse results in mice colonic microbiome composition. The core reason for these differences lies in the selective pressure exerted by each treatment on the microbial community. AVHS@RWWRWW likely acts as a targeted antimicrobial peptide, specifically inhibiting pathogens while sparing beneficial bacteria, like *Bifidobacterium globosum*. This may free up ecological niches for these beneficial taxa to thrive. In contrast, both the broad-spectrum antimicrobial peptide LL-37 and the potent disinfectant CHX act non-specifically. Their indiscriminate killing disrupts the entire microbial ecosystem, creating vacant niches that are rapidly colonized by inherently resistant or fast-recovering opportunistic pathogens, such as *Clostridioides difficile*, and bacteria with high antibiotic resistance genes, including many within the Bacteroidota and Proteobacteria phyla. The phylum-level similarity of some groups to the control masks significant species-level changes, highlighting that a seemingly similar overall structure can harbor critically different and potentially pathogenic members.

The current study still has some limitations. Firstly, the native form of AVHS showed limited efficacy in both antibacterial and remineralization functions. To address these limitations and enhance its therapeutic potential, we implemented structural modifications to optimize its biological activity and expand its clinical applications. Secondly, while our study provides initial insights, the comparative analysis of AVHS@RWWRWW's efficacy, safety, and mechanism relative to those of existing agents remains limited. Therefore, future studies should include more comprehensive comparisons. Thirdly, although our case-control study identified AVHS as a "predominant metabolite" associated with a caries-free state, we acknowledge that the case-control design inherently limits causal inferences regarding the relationship between AVHS and caries prevention. Crucial questions remain—specifically, its precise origin and functional role, and whether it is an active metabolite or a degradation byproduct. Future well-designed randomized controlled trials or cohort studies with the targeted omics tests and laboratory studies would be needed to further confirm the origins and functional role of AVHS.

5. Conclusions

This study identified Ala-Val-His-Ser (AVHS) as the predominant metabolite, demonstrating excellent biocompatibility, significant inhibition of *S. mutans* growth and acid production, and remarkable biofilm-targeting capability *in vitro*. AVHS@RWWRWW exhibited substantially enhanced therapeutic potential, superior anti-biofilm activity and caries-preventive effects, making it a promising antimicrobial agent for oral health applications.

Author contributions

Yuan-Meng Yang and Teck-Ek Ho: conceptualization, investigation, formal analysis, visualization, and writing – original draft;

Wen-Jia Gu: methodology, validation, resources, and data curation; Fei Li: conceptualization, methodology, data curation, and investigation; Edward Chin Man Lo: conceptualization, methodology, and resources, supervision; Jian-Shu Li: conceptualization and methodology; Jun Luo: methodology and investigation; Qi Chen: data curation and visualization; Lin-Lu Dai: writing – review & editing and supervision; May Lei Mei: conceptualization and methodology; Wen-Jie Zhang and Hai-Xia Lu: conceptualization, methodology, validation, writing – review & editing, supervision, and funding acquisition. All authors gave final approval and agree to be accountable for all aspects of the work.

Conflicts of interest

The authors declare no competing interests or personal relationships that could have appeared to influence the work reported in this paper.

Data availability

The datasets used or analyzed during the present study are available from the corresponding author upon reasonable request.

Acknowledgements

This study was supported by grants from the Hong Kong Macao Taiwan Science and Technology Cooperation Project of Shanghai Municipal Science and Technology Commission (Project No. 22410760200) and Opening Research Fund from Shanghai Key Laboratory of Stomatology, Shanghai Ninth People's Hospital, College of Stomatology, Shanghai Jiao Tong University School of Medicine (Project No. 2022SKLS-KFKT010).

References

1 M. O. Folayan, M. El Tantawi, F. Ramos-Gomez and W. Sabbah, *Front. Public Health*, 2020, **8**, 141.
2 J. Zou, Q. Du, L. Ge, J. Wang, X. Wang, Y. Li, G. Song, W. Zhao, X. Chen, B. Jiang, Y. Mei, Y. Huang, S. Deng, H. Zhang, Y. Li and X. Zhou, *Int. J. Oral Sci.*, 2022, **14**, 35.
3 P. P. Y. Lam, H. Chua, M. Ekambaram, E. C. M. Lo and C. K. Y. Yiu, *J. Evid. Based Dent. Pract.*, 2022, **22**, 101732.
4 P. Phantumvanit, Y. Makino, H. Ogawa, A. Rugg-Gunn, P. Moynihan, P. E. Petersen, W. Evans, C. A. Feldens, E. Lo, M. H. Khoshnevisan, R. Baez, B. Varenne, T. Vichayanrat, Y. Songpaisan, M. Woodward, S. Nakornchai and C. Ungchusak, *Community Dent. Oral Epidemiol.*, 2018, **46**, 280–287.
5 W. K. Seow, *Pediatr. Clin. North Am.*, 2018, **65**, 941–954.
6 S. S. Garcia, M. S. Blackledge, S. Michalek, L. Su, T. Ptacek, P. Eipers, C. Morrow, E. J. Lefkowitz, C. Melander and H. Wu, *J. Dent. Res.*, 2017, **96**, 807–814.
7 N. Takahashi and B. Nyvad, *J. Dent. Res.*, 2011, **90**, 294–303.
8 N. Takahashi, *J. Dent. Res.*, 2015, **94**, 1628–1637.
9 R. J. Lamont, H. Koo and G. Hajishengallis, *Nat. Rev. Microbiol.*, 2018, **16**, 745–759.
10 N. Takahashi and T. Sato, *J. Dent. Res.*, 2001, **80**, 1425–1429.
11 N. Takahashi and T. Sato, *Oral Microbiol. Immunol.*, 2002, **17**, 50–54.
12 J. Washio, T. Ogawa, K. Suzuki, Y. Tsukiboshi, M. Watanabe and N. Takahashi, *Biomed. Res.*, 2016, **37**, 251–257.
13 M. Agnello, L. Cen, N. C. Tran, W. Shi, J. S. McLean and X. He, *J. Dent. Res.*, 2017, **96**, 924–930.
14 M. M. Nascimento, Y. Liu, R. Kalra, S. Perry, A. Adewumi, X. Xu, R. E. Primosch and R. A. Burne, *J. Dent. Res.*, 2013, **92**, 604–608.
15 M. López-Ruiz, F. Navas, P. Fernández-García, S. Martínez-Erro, M. V. Fuentes, I. Giráldez, L. Ceballos, C. M. Ferrer-Luque, M. Ruiz-Linares, V. Morales, R. Sanz and R. A. García-Muñoz, *J. Nanobiotechnol.*, 2022, **20**, 502.
16 M. M. Nascimento, E. Zaura, A. Mira, N. Takahashi and J. M. Ten Cate, *J. Dent. Res.*, 2017, **96**, 733–740.
17 A. Schulz, R. Lang, J. Behr, S. Hertel, M. Reich, K. Kümmerer, M. Hannig, C. Hannig and T. Hofmann, *Sci. Rep.*, 2020, **10**, 697.
18 O. L. Zhang, J. Y. Niu, O. Y. Yu, M. L. Mei, N. S. Jakubovics and C. H. Chu, *Int. J. Mol. Sci.*, 2023, **24**(4), 4247.
19 R. E. W. Hancock, M. A. Alford and E. F. Haney, *Nat. Rev. Microbiol.*, 2021, **19**, 786–797.
20 A. R. P. Silva, M. S. Guimarães, J. Rabelo, L. H. Belén, C. J. Perecin, J. G. Farías, J. H. P. M. Santos and C. O. Rangel-Yagui, *J. Mater. Chem. B*, 2022, **10**, 3587–3600.
21 J. Y. Niu, I. X. Yin, M. L. Mei, W. K. K. Wu, Q.-L. Li and C. H. Chu, *Mol. Oral Microbiol.*, 2021, **36**, 159–171.
22 A. Aidoukovitch, E. Bankell, J. R. Davies and B.-O. Nilsson, *Acta Odontol. Scand.*, 2021, **79**, 466–472.
23 S. Joly, C. Maze, P. B. McCray and J. M. Guthmiller, *J. Clin. Microbiol.*, 2004, **42**, 1024–1029.
24 A. I. Gomaa, C. Martinent, R. Hammami, I. Fliss and M. Subirade, *Front. Chem.*, 2017, **5**, 103.
25 Á. Martin-Serrano, R. Gómez, P. Ortega and F. J. de la Mata, *Pharmaceutics*, 2019, **11**(9), 448.
26 N. K. Brogden and K. A. Brogden, *Int. J. Antimicrob. Agents*, 2011, **38**, 217–225.
27 Y. Gao, H. Fang, L. Fang, D. Liu, J. Liu, M. Su, Z. Fang, W. Ren and H. Jiao, *Curr. Pharm. Des.*, 2018, **24**, 904–910.
28 R. Li, J. Mao, P. Zheng, R. Wang, Z. Yang and S. Qian, *World J. Microbiol. Biotechnol.*, 2023, **40**, 1.
29 J. Huang, Y. Xu, Y. Xue, Y. Huang, X. Li, X. Chen, Y. Xu, D. Zhang, P. Zhang, J. Zhao and J. Ji, *Nat. Biomed. Eng.*, 2023, **7**, 797–810.
30 W. N. Addison, S. J. Miller, J. Ramaswamy, A. Mansouri, D. H. Kohn and M. D. McKee, *Biomaterials*, 2010, **31**, 9422–9430.
31 J. D. Hartgerink, E. Beniash and S. I. Stupp, *Science*, 2001, **294**, 1684–1688.
32 T. E. H. Y. Yang and E. C. M. Lo, *et al.*, *Shanghai J. Stomatol.*, 2024, **33**(5), 492–499.
33 E. von Elm, D. G. Altman, M. Egger, S. J. Pocock, P. C. Gøtzsche and J. P. Vandenbroucke, *Lancet*, 2007, **370**, 1453–1457.

34 Z. Pang, G. Zhou, J. Ewald, L. Chang, O. Hacariz, N. Basu and J. Xia, *Nat. Protoc.*, 2022, **17**, 1735–1761.
35 N. B. Pitts and K. R. Ekstrand, *Community Dent. Oral Epidemiol.*, 2013, **41**, e41–e52.
36 I. P. Sæbø, M. Bjørås, H. Franzyk, E. Helgesen and J. A. Booth, *Int. J. Mol. Sci.*, 2023, **24**(3), 2914.
37 Z. Zhang, Y. Shi, H. Zheng, Z. Zhou, Z. Wu, D. Shen, Y. Wang, Y. Zhang, Z. Wang and B. Fu, *Int. J. Nanomed.*, 2021, **16**, 7623–7637.
38 P. H. Keyes, *J. Dent. Res.*, 1958, **37**, 1088–1099.
39 A. M. Katz and F. C. Messineo, *Circ. Res.*, 1981, **48**(1), 1–16.
40 N. Joudeh and D. Linke, *J. Nanobiotechnol.*, 2022, **20**, 262.
41 L. C. Gomes and F. J. Mergulhão, *Scanning*, 2017, **2017**, 2960194.
42 S. Bröer and G. Gauthier-Coles, *J. Nutr.*, 2022, **152**, 16–28.
43 T. R. Ribeiro, K. J. Dria, C. B. M. de Carvalho, A. J. Monteiro, M. C. Fonteles, K. de Moraes Carvalho and C. S. R. Fonteles, *Int. J. Paediatr. Dent.*, 2013, **23**, 225–234.
44 J. D. Rudney, P. D. Jagtap, C. S. Reilly, R. Chen, T. W. Markowski, L. Higgins, J. E. Johnson and T. J. Griffin, *Microbiome*, 2015, **3**, 69.
45 X. Gao, S. Jiang, D. Koh and C.-Y. S. Hsu, *Periodontol 2000*, 2016, **70**, 128–141.
46 M. Ayad, B. C. Van Wuyckhuyse, K. Minaguchi, R. F. Raubertas, G. S. Bedi, R. J. Billings, W. H. Bowen and L. A. Tabak, *J. Dent. Res.*, 2000, **79**, 976–982.
47 K. R. Sims, J. P. Maceren, Y. Liu, G. R. Rocha, H. Koo and D. S. W. Benoit, *Acta Biomater.*, 2020, **115**, 418–431.
48 J. Moon, K. Seo and J.-S. Kwon, *npj Biofilms Microbiomes*, 2025, **11**, 65.
49 P. S. Sheet, S. Park, A. T. Nguyen, S. George, C. Maier and D. Koley, *Anal. Chim. Acta*, 2024, **1321**, 343042.
50 D. F. Williams, *Med. Prog. Technol.*, 1976, **4**, 31–42.
51 I. Struzycka, *Pol. J. Microbiol.*, 2014, **63**, 127–135.
52 J. A. Lemos, S. R. Palmer, L. Zeng, Z. T. Wen, J. K. Kajfasz, I. A. Freires, J. Abranches and L. J. Brady, *Microbiol. Spectr.*, 2019, 7(1), DOI: **10.1128/microbiolspec.gpp3-0051-2018**.
53 L. Chen, B. Chakraborty, J. Zou, R. A. Burne and L. Zeng, *Appl. Environ. Microbiol.*, 2019, **85**(10), e00370-19.
54 Y. Shen, F. Yu, L. Qiu, M. Gao, P. Xu, L. Zhang, X. Liao, M. Wang, X. Hu, Y. Sun and Y. Pan, *Front. Cell. Infect. Microbiol.*, 2022, **12**, 1106392.
55 N. S. Jakubovics, S. D. Goodman, L. Mashburn-Warren, G. P. Stafford and F. Cieplik, *Periodontol 2000*, 2021, **86**, 32–56.
56 D. S. W. Benoit, K. R. Sims and D. Fraser, *ACS Nano*, 2019, **13**, 4869–4875.
57 X. Li, Y.-C. Yeh, K. Giri, R. Mout, R. F. Landis, Y. S. Prakash and V. M. Rotello, *Chem. Commun.*, 2015, **51**, 282–285.
58 B. Li, J. Mao, J. Wu, K. Mao, Y. Jia, F. Chen and J. Liu, *Small*, 2024, **20**, e2306135.
59 H. Milly, F. Festy, M. Andiappan, T. F. Watson, I. Thompson and A. Banerjee, *Dent. Mater.*, 2015, **31**, 522–533.
60 K. Yamaguchi, M. Miyazaki, T. Takamizawa, H. Inage and B. K. Moore, *J. Dent.*, 2006, **34**, 230–236.
61 T. Bjarnsholt, K. Buhlin, Y. F. Dufrêne, M. Gomelsky, A. Moroni, M. Ramstedt, K. P. Rumbaugh, T. Schulte, L. Sun, B. Åkerlund and U. Römling, *J. Intern. Med.*, 2018, **284**, 332–345.
62 R. M. Donlan, *Clin. Infect. Dis.*, 2011, **52**, 1038–1045.
63 J. W. Costerton, P. S. Stewart and E. P. Greenberg, *Science*, 1999, **284**, 1318–1322.
64 S. S. Socransky and A. D. Haffajee, *Periodontol 2000*, 2002, **28**, 12–55.
65 Z. Yin, Y. Liu, A. Anniwaer, Y. You, J. Guo, Y. Tang, L. Fu, L. Yi and C. Huang, *Adv. Mater.*, 2023, e2305633, DOI: **10.1002/adma.202305633**.
66 H. Anwar, M. Dasgupta, K. Lam and J. W. Costerton, *J. Antimicrob. Chemother.*, 1989, **24**, 647–655.
67 M. R. Brown, D. G. Allison and P. Gilbert, *J. Antimicrob. Chemother.*, 1988, **22**, 777–780.
68 W. W. Nichols, M. J. Evans, M. P. Slack and H. L. Walmsley, *J. Gen. Microbiol.*, 1989, **135**, 1291–1303.
69 K. Lewis, *Cell*, 2020, **181**, 29–45.
70 S. J. Ford, *Int. J. Surg.*, 2008, **6**, 418–419.
71 L. Breschi, T. Maravic, A. Comba, S. R. Cunha, A. D. Loguercio, A. Reis, V. Hass, M. Cadenaro, E. Mancuso, E. Mayer-Santos, L. Niu, D. H. Pashley, F. R. Tay and A. Mazzoni, *Dent. Mater.*, 2020, **36**, 672–680.
72 A. D. Haffajee, R. P. Teles, M. R. Patel, X. Song, N. Veiga and S. S. Socransky, *J. Periodontal Res.*, 2009, **44**, 511–519.

